Weyl Semimetal to Metal Phase Transitions Driven by Quasiperiodic Potentials

J. H. Pixley,[1,2] Justin H. Wilson,[3] David A. Huse,[4] and Sarang Gopalakrishnan[5]
[1]Department of Physics and Astronomy, Center for Materials Theory, Rutgers University, Piscataway, New Jersey 08854, USA
[2]Condensed Matter Theory Center and the Joint Quantum Institute, Department of Physics, University of Maryland, College Park, Maryland 20742-4111, USA
[3]Institute of Quantum Information and Matter and Department of Physics, California Institute of Technology, Pasadena, California 91125, USA
[4]Physics Department, Princeton University, Princeton, New Jersey 08544, USA
[5]Department of Engineering Science and Physics, CUNY College of Staten Island, Staten Island, New York 10314, USA and Initiative for the Theoretical Sciences, CUNY Graduate Center, New York, New York 10016 USA

(Received 23 February 2018; published 18 May 2018)

We explore the stability of three-dimensional Weyl and Dirac semimetals subject to quasiperiodic potentials. We present numerical evidence that the semimetal is stable for weak quasiperiodic potentials, despite being unstable for weak random potentials. As the quasiperiodic potential strength increases, the semimetal transitions to a metal, then to an "inverted" semimetal, and then finally to a metal again. The semimetal and metal are distinguished by the density of states at the Weyl point, as well as by level statistics, transport, and the momentum-space structure of eigenstates near the Weyl point. The critical properties of the transitions in quasiperiodic systems differ from those in random systems: we do not find a clear critical scaling regime in energy; instead, at the quasiperiodic transitions, the density of states appears to jump abruptly (and discontinuously to within our resolution).

DOI: 10.1103/PhysRevLett.120.207604

Disorder qualitatively modifies the properties of materials in contexts ranging from spin glasses [1] to the quantum Hall effect [2]. A striking consequence of disorder in quantum systems is the localization of excitations [3] and the resulting lack of transport [4,5]. While disorder causes localization, it is not a *necessary* condition for localization: deterministic quasiperiodic potentials (QPs) can also support localized excitations [6,7] but differ from uncorrelated disorder in at least two crucial respects. First, QPs have stable delocalized states even in one dimension [6,7] and (unlike disordered systems in any dimension) can exhibit ballistic transport [8]. Second, QPs lack large-scale fluctuations, so the rare-region "Griffiths" effects that sometimes dominate the behavior of disordered systems [9,10] are absent. These distinctions are of practical relevance, since experiments with ultracold atoms often use quasiperiodic potentials as an easy-to-implement proxy for randomness [11].

The present work addresses a system in which the distinction between quasiperiodicity and randomness is central, specifically, Weyl semimetals [12] subject to QPs. In the *random* case, transport at energies near $E = 0$ (i.e., the Weyl point) is anomalous because of the interplay between disorder and the vanishing density of states (DOS) [13–38]. Disorder is perturbatively irrelevant at the Weyl points [13], suggesting that the ballistic semimetal should be stable to weak disorder (see Ref. [39] for a recent review from this perspective). However, rare-region effects fill in the zero-energy DOS and destabilize the semimetal for infinitesimal disorder [18,32,38], although the (so-called) avoided quantum critical point separating the semimetal from the diffusive metal persists as a crossover [32,33,36,37]. The random potential is both the control parameter for the avoided phase transition and the source of rare regions that destabilize it. To disaggregate these effects, we consider QPs, which lack rare regions. Note that an analogous situation occurs for many-body localization: disorder both drives localization and (through rare-region effects) destabilizes it [40]. The present system potentially offers a more tractable setting with similar phenomena.

For QPs, we find two types of phases: (i) a semimetal at weak QP strength with ballistic wave functions and a vanishing $E = 0$ DOS, and (ii) a diffusive metal at stronger QPs. (We also find an Anderson localized phase for much stronger QPs, but will not focus on the localized phase here.) We present evidence that the semimetal-to-metal transition in this case is sharp and not avoided; its critical properties differ from those of the avoided critical point in the random case. We find a rich phase diagram, featuring a "miniband inversion" transition within the semimetal phase, at which the negative and positive energy states near the Weyl points cross in energy; this crossing is associated with an additional pair of ballistic-to-diffusive transitions around $E = 0$.

Model, methods, observables.—We focus on a three-dimensional model on a simple cubic lattice that represents an inversion-symmetry broken Weyl semimetal

$$H = \sum_{\mathbf{r},\mu=x,y,z} \frac{1}{2}(it_\mu \psi^\dagger_{\mathbf{r}} \sigma_\mu \psi_{\mathbf{r}+\hat{\mu}} + \text{H.c.}) + \sum_{\mathbf{r}} \psi^\dagger_{\mathbf{r}} V(\mathbf{r}) \psi_{\mathbf{r}}. \quad (1)$$

$\psi_{\mathbf{r}}$ is a two-component spinor, σ_μ are the Pauli operators, and the onsite quasiperiodic potential (QP) is $V(\mathbf{r})$. We take a three-dimensional QP (diagonal in spinor space) $V(\mathbf{r}) = \sum_{\mu=x,y,z} W_\mu \cos(Q_L r_\mu + \phi_\mu)$, where each ϕ_μ is a random phase sampled between $[0, 2\pi]$ that is the same at every site (for the case of a one-dimensional QP, see Ref. [41]). We will also consider the randomized version of the QP potential in which the ϕ_μ are random at each lattice site [42]. This allows us to compare results between these two models at the same W since each site has the same distribution of potentials. We consider twisted boundary conditions $t_\mu = |t_\mu| \exp(i\theta_\mu/L)$, where θ_μ is randomly sampled between $[0, 2\pi]$. The linear system size is taken to be a Fibbonaci number $L = F_n$ with a wave vector $Q_L = 2\pi F_{n-2}/L$; as $n \to \infty$, $Q_L/2\pi \to 4/(\sqrt{5}+1)^2$. We average over random twists and phases; we present results averaged over 200–1000 samples.

We consider two slightly distinct models. To locate the critical points in the DOS, we make the simplest choice and set $|t_\mu| = 1$, $|W_\mu| = W$. However, to prevent the threefold symmetry of this model from contaminating level statistics, we study level statistics for an *anisotropic* model, with broken symmetry in the hopping and potential; here we take $|t_x| = 1$, $|t_y| = 0.9$, $|t_z| = 1.1$, $|W_x| = W$, $|W_y| = 0.95W$, $|W_z| = 1.1W$. The models show similar critical behavior, though the (nonuniversal) critical W differs slightly.

We use a combination of numerically exact techniques to explore Eq. (1). To compute the DOS for large systems we use the kernel polynomial method [43] (KPM). The DOS is

$$\rho(E) = [L^{-3} \sum_i \delta(E - E_i)], \quad (2)$$

where E_i is the ith eigenstate, $[\ldots]$ denotes a sample average, and L is the linear system size. The KPM expands the DOS in Chebyshev polynomials to order N_C, which is a proxy for energy resolution. We also directly compute the second derivative $\rho''(0)$ with KPM [33]; we expect $\rho''(0)$ to be singular at the semimetal-to-metal transition.

To study level statistics and wave functions we use exact diagonalization. For level statistics we compute the adjacent gap ratio

$$r_i \equiv \min(\delta_i, \delta_{i+1})/\max(\delta_i, \delta_{i+1}), \quad (3)$$

where $\delta_i = E_i - E_{i-1}$ and the eigenvalues have been sorted in ascending order $E_1 < E_2 < \ldots < E_N$. Another metric we use is the momentum-space inverse participation ratio (IPR):

$$\mathcal{I}_k(E) \equiv \left(\sum_{\mathbf{k}} |\psi_E(\mathbf{k})|^2\right)^{-2} \sum_{\mathbf{k}} |\psi_E(\mathbf{k})|^4. \quad (4)$$

This quantity probes how much the eigenfunction ψ_E at energy E resembles a plane wave. The ballistic phase is localized in momentum space and thus $\mathcal{I}_k$ is L independent, whereas in the diffusive phase the wave function is spread out in $\mathbf{k}$ and $\mathcal{I}_k \to 0$ with increasing L.

We have also computed transport properties [44], but our results on transport at the transition are inconclusive. We use KPM to compute the dynamics of an initially localized wave packet [45]; however, a localized initial state has little weight near the Weyl points and is largely insensitive to the transitions studied here. To focus on behavior near the Weyl points, we have also computed energy-resolved spectral functions of the local density-density correlation function using exact diagonalization; however, the system sizes accessible here are sufficiently small ($L = 13$) that our results are likely severely contaminated by finite size effects.

Phase diagram.—We begin by discussing the phase diagram of the model in Eq. (1) as a function of energy (E) and QP strength (W) [Fig. 1]. Unlike disorder, the QP gives rise to an intricate energy-level structure, with mini-bands and hard gaps forming even at relatively weak QP strength [Fig. 1(a)]. The main features are evident in the color plots of the DOS [Fig. 1(b)] and level statistics [Fig. 1(c)] as a function of E and W.

For small W and $E \approx 0$, the quasiperiodic system behaves like the clean system: the DOS vanishes

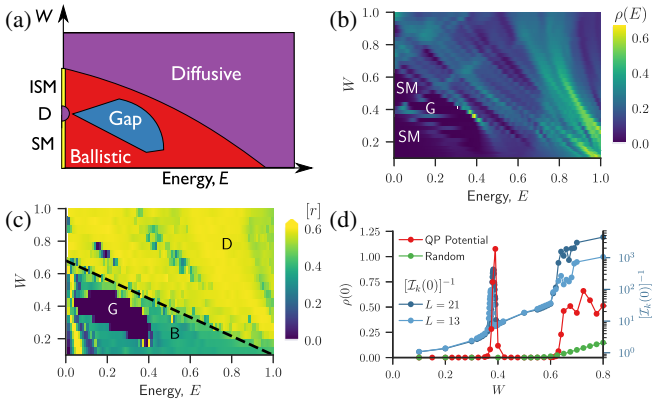

FIG. 1. (a) Schematic phase diagram in energy (E) and QP potential strength (W). We have labeled the diffusive (D), ballistic (B), gapped (G), inverted semimetal (ISM), and semimetal (SM) phases. (b) Density of states (DOS) in the $|E| - W$ plane computed using KPM for $L = 55$ and $N_C = 2^{10}$, color represents DOS. (c) Level statistics in the $|E| - W$ plane computed from exact diagonalization for $L = 13$. The color denotes the average adjacent gap ratio Eq. (3). (d) Average zero energy DOS $\rho(0)$ versus W for $L = 144$ and $N_C = 2^{10}$, from KPM (left vertical axis) as well as the momentum-space IPR $\mathcal{I}_k(E)$ for the state closest to zero energy, computed for $L = 13$, 21 using Lanczos (right vertical axis).

quadratically at $E = 0$ and all states remain ballistic (i.e., localized in momentum space). As W is increased, states far away from $E = 0$ delocalize in momentum space and develop random-matrix level statistics; we call these energy regimes "diffusive" (by analogy with the disordered system). At $W \approx 0.15$, minibands around $E = 0$ separate themselves from higher-energy states, and a hard gap appears between the miniband and the higher energy states; we return to this effect below. As W is increased, the positive- and negative-energy minibands merge at $W_m/t = 0.380 \pm 0.001$ at $E = 0$ (giving rise to an intermediate, apparently diffusive, metallic phase for $W_m < W \lesssim 0.395t$) and then *cross*: the positive and negative energy minibands change places, and an "inverted" semimetal forms [44]. As W increases further, the semimetallic region disappears again at $W_c \approx 0.6345 \pm 0.001$. For $W \gtrsim W_c$, the DOS at $E = 0$ is finite and wave packet dynamics are diffusive [44]. W_c in this quasiperiodic model is close to the avoided critical point at $W \approx 0.625$ in the equivalent random model (i.e., the model with random phases at each site in the potential). Level statistics and momentum-space IPR approximately track the DOS: high-DOS regions are typically diffusive and low-DOS regions typically ballistic.

Critical properties at W_c.—We now discuss the critical properties of the transition at W_c (Fig. 2). The DOS near $E = 0$, on the semimetallic side ($0.395t < W < W_c$), goes like $\rho(E) \sim E^2$ and very close to W_c we find $\rho(E) \sim E^2(W_c - W)^{-\beta}$, with $\beta = 2 \pm 0.8$. On the "metallic" side, the DOS grows rapidly, but we cannot resolve a clear power-law regime. In addition, the crossover energy scale at which the low-energy $\rho(E) \sim E^2$ behavior ends appears to shrink linearly with $W_c - W$. Unlike the random model, which has a clear critical energy window for which $\rho(E) \sim |E|$, the quasiperiodic model shows no clear scaling other than $\rho(E) \sim E^2$ at the lowest energies in the semimetal. The simplest way to account for these observations is if the critical point itself has a nonzero DOS; i.e., at $E = 0$ in the infinite system the DOS is discontinuous at the transition. Our observations are consistent with this scenario; however, it remains possible that the zero-energy DOS instead grows continuously but extremely rapidly.

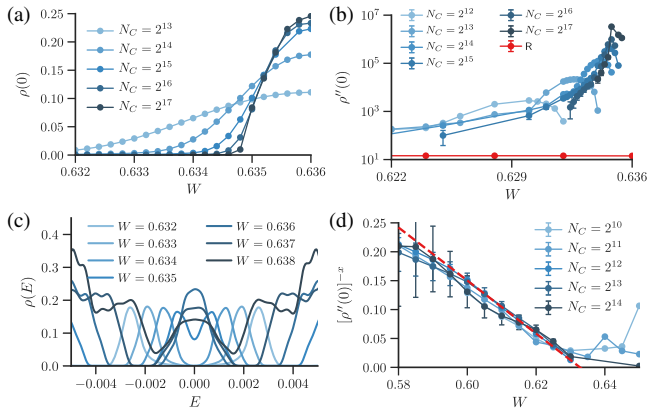

FIG. 2. Critical behavior of the DOS. (a) $\rho(E = 0)$ vs W with $L = 55$, near the transition at $W_c \approx 0.63$; for various KPM expansion orders N_C, (i.e., different energy resolution). (b) Second derivative of the DOS, $\rho''(E = 0)$, vs W with $L = 55$, for various N_C; $\rho''(0)$ rises steeply with N_C, and does not saturate. The black solid line is the data for the equivalent random model (there is a broad peak near $W \approx 0.625$ that looks flat on this scale). (c) $\rho(E)$ versus E across the transition, at fixed $L = 55$, $N_C = 2^{16}$. (d) The stability of the scaling regime in $\rho''(E = 0)^{-x}$ versus W with N_C and $L = 89$ for $x = 0.5$ indicating that $\rho''(E = 0) \sim (W_c - W)^{-2}$, (dashed black line is a linear fit to the data with $N_C = 2^{12}$).

To identify the nonanalyticity of the DOS at W_c we study the dependence of $\rho''(0)$ on expansion order. For each choice of $N_C \leq 2^{14}$ we converge our data for $\rho(0)$ and $\rho''(0)$ in L so that we know the only rounding is due to N_C [44]; however, for $N_C > 2^{15}$ it is infeasible to converge with L, so our data are rounded by both N_C and L. The divergence of $\rho''(0)$ in Fig. 2(b) is striking, reaching $\rho''(0) \sim 10^7$ at $N_C = 2^{17}$, with no sign of saturation. By contrast, in the random problem, the maximum observed $\rho''(0)$ at the avoided transition is $\sim 10^3$ (where the peak value was close to saturating) [33]. Thus, the transition in the present case appears to be sharp and not avoided. This is consistent with the absence of rare regions and the stability of the ballistic phase, two properties that are common in quasiperiodic systems generally [46].

Wave functions and level statistics.—The DOS does not directly tell us whether the system is ballistic or diffusive; a better probe is the level statistics, which we probe via the adjacent gap ratio r [Eq. (3)]. In the ballistic regime, states are localized in momentum space so we expect Poisson level statistics ($[r] \approx 0.39$); in the diffusive regime, we expect random-matrix behavior, which (for twisted boundary conditions that breaks time-reversal symmetry) should follow the Gaussian unitary ensemble (GUE) ($[r] \approx 0.60$). We see the limiting behaviors at small and large W; at moderate $W \gtrsim 0.1$ states away from $E = 0$ are mostly diffusive. Near W_c, the level statistics cross over from Poisson-like to GUE-like, though at the accessible system sizes $L = 13$, the level statistics near $E = 0$ is intermediate between Poisson and GUE throughout the transition regime. There is considerable inhomogeneity in the level statistics even in the narrow window near zero energy (see Figs. 3 and 4); notably, at least at the accessible system sizes, states near $E = 0$ appear more random-matrix like than higher-DOS regions further from zero energy. The momentum-space IPR tracks r, exhibiting similar heterogeneity; throughout the semimetallic phase, zero-energy states are more tightly localized in momentum space than those away from zero energy. Using the Lanczos method, we have explored the spread of IPR for slightly larger systems ($L = 21$); the heterogeneity is more pronounced, but the trend is similar [44]. In general our results suggest that there is a momentum-space delocalization transition that coincides with the DOS transition.

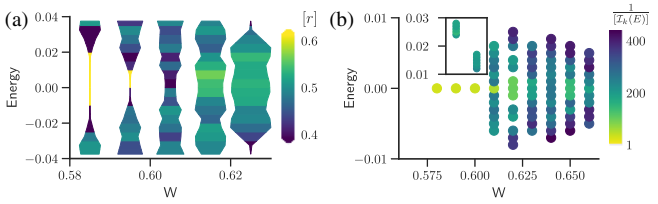

FIG. 3. Level statistics and momentum-space IPR for $L = 13$ systems near W_c; for this system size $W_c \approx 0.61$ averaged over 400 samples. Left: a color plot of $\langle r \rangle$ vs E and W; the color indicates the gap ratio (3) in an energy bin, and the size of a dot indicates the DOS in that bin. Right: Momentum-space IPR vs E and W; lowest 10 eigenvalues averaged over 100 realizations; inset shows the same quantity at a higher energy range for the W value the inset is above.

Miniband transition.—We now turn to the physics at $W < W_c$ (as shown in Fig. 4), and discuss some of the fine structure seen inside the semimetal, particularly the miniband inversion transition. This fine structure is absent in disordered systems. We first discuss the origin of these minibands, which can be understood using perturbation theory in the QP. The band structure of the clean system consists of eight Weyl points at $(0,0,0), (0,0,\pi), (0,\pi,0), \ldots, (\pi,\pi,\pi)$; for states near the Weyl points, energies are set by the distance in momentum space from the Weyl point. The QP transfers momentum $\sim 0.76\pi$. Thus, the QP can hybridize a state at $(0.12\pi, 0, 0)$ with one at $(\pi - 0.12\pi, 0, 0)$, and so on [see Fig. 4(b)]. Since these degenerate states belong to Weyl cones with opposite chirality, and are on opposite sides of their Weyl cones, they have the same spin structure and can mix.

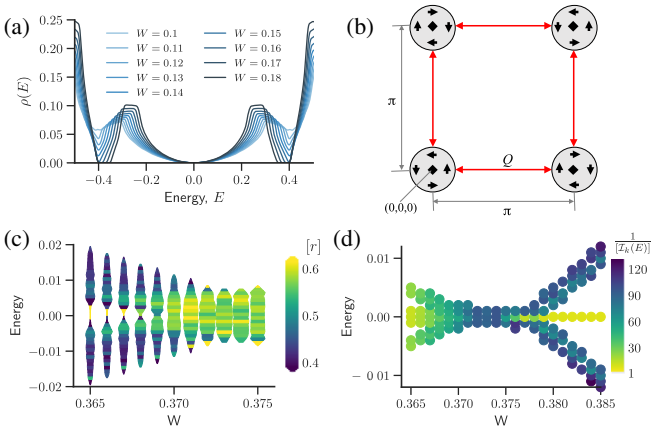

FIG. 4. Formation of the miniband and its phase transition. (a) DOS vs E at various small $W \approx 0.15$, showing how the miniband detaches from the other states as W increases. (b) Perturbative structure of the miniband: it forms because the QP hybridizes states from different Weyl cones. Circles denote equal-energy contours in the clean system; thick arrows denote spin textures. (c) Level statistics [Eq. (3)], vs E and W, near the miniband transition, for $L = 13$. (d) Momentum-space IPR [Eq. (4)], vs E and W, near the miniband transition, for $L = 13$ (lowest 10 eigenstates pictured).

As the potential becomes stronger, less precisely degenerate states hybridize and this hybridization opens up a gap, separating states that are close to the Weyl nodes (the "miniband") from the rest of the band.

Our exact diagonalization results on $L = 13$ fit this picture. The quasiperiodic approximant for this L has a wave vector $Q_L = 2\pi(5/13)$. The estimate above for the characteristic wave vector of the miniband suggests that only states with momenta within $(0.5/13) \times 2\pi$ of a Weyl point will contribute to the miniband. There are 54 such states. A miniband consisting of these 54 states forms at $W \approx 0.15$ [see Fig. 4(a)]; the miniband is separated from other states by a hard gap.

After the miniband forms, it flattens with increasing W, until at $W = W_m \approx 0.38$ the DOS at $E = 0$ fills in (note that for $L = 13$ the apparent $W_m \approx 0.371$ while at $L = 21$, $W_m \approx 0.378$); $\rho(E)$ becomes nonanalytic with a divergence on approach to W_m from both sides, $\rho''(0) \sim |W - W_m|^{-\beta}$ with $\beta = 2 \pm 0.6$ [44]. The critical properties of the DOS at this transition are apparently similar to those at W_c, but the transition in the level statistics is clearer in this case [compare Figs. 3(a) and 4(c)]. As one approaches the transition, states near the Weyl point cross over to random-matrix level statistics. Again, the filling in of the DOS at $E = 0$ coincides (to within our resolution) with the appearance of diffusive states at $E = 0$. As one increases W past this point, the minibands separate out and invert, and their states once again become ballistic. This behavior is again what one would expect perturbatively: the QP mixes states in the miniband with one another only at high orders in perturbation theory, whereas the leading order effect is for each positive (negative) energy state to be pushed down (up) as W increases, leading to an inversion. This inversion is driven by Q_L connecting nodes at leading order in perturbation theory; for a smaller Q_L whose leading effect is only intranode hybridization, the inversion disappears [44].

Discussion.—We have provided evidence that Weyl and Dirac semimetals subject to quasiperiodic potentials undergo a true quantum phase transition between a ballistic phase with vanishing DOS at $E = 0$ and a diffusive phase with nonvanishing DOS at $E = 0$. We see no indications that the critical point is avoided: the DOS appears nonanalytic, with no sign of intrinsic rounding. The transition affects the DOS, level statistics, and wave function structure at once, to within our resolution. That these should coincide is not *a priori* obvious; a ballistic phase with nonzero DOS at $E = 0$ is possible in principle, and would seem natural at sufficiently low DOS. The numerical evidence, however, suggests a discontinuous or at least a very steep rise of the DOS at the transition. In further contrast to the random case, the DOS lacks a critical energy window. In addition to this transition, we found a range of phenomena at weaker quasiperiodic potentials, including the formation of minibands and hard band gaps, and a pair of semimetal-to-metal transitions at which the positive and

negative energy minibands merge and go through each other. These miniband transitions are natural in quasiperiodic systems, but their precise location depends on the wave vector Q_L.

The most natural experimental settings for exploring the effects studied here are ultracold gases, where Weyl points have already been introduced [47–50]. The semimetal-to-metal transition can be readily studied in such systems by standard spectroscopic methods (which reveal the DOS) or time-of-flight imaging: the momentum distributions of the ballistic and diffusive phases will be quite different. Such systems also offer the possibility of studying interaction effects in Weyl semimetals, and their interplay with quasiperiodic potentials.

We thank Trithep Devakul for useful discussions and Elio König for comments on a draft. The authors are grateful for support from the Laboratory for Physical Sciences (J. P.), the Air Force Office for Scientific Research (J. W.), and the NSF under DMR-1653271 (S. G.). J. P. acknowledges the Aspen Center for Physics where some of this work was performed, which is supported by National Science Foundation Grant No. PHY-1607611. The authors acknowledge the University of Maryland supercomputing resources, the Beowulf cluster at the Department of Physics and Astronomy of Rutgers University, and the Office of Advanced Research Computing (OARC) at Rutgers, The State University of New Jersey for providing access to the Amarel cluster and associated research computing resources that have contributed to the results reported here.

[1] K. Fischer and J. Hertz, Spin-Glasses, *Cambridge Studies in Magnetism* (Cambridge University Press, Cambridge, England, 1991), Vol. I.
[2] R. E. Prange and S. M. Girvin, The Quantum Hall Effect, *Graduate Texts in Contemporary Physics* (Springer, New York, 1987).
[3] P. W. Anderson, Phys. Rev. **109**, 1492 (1958).
[4] P. A. Lee and T. V. Ramakrishnan, Rev. Mod. Phys. **57**, 287 (1985).
[5] R. Nandkishore and D. A. Huse, Annu. Rev. Condens. Matter Phys. **6**, 15 (2015).
[6] M. Y. Azbel, Phys. Rev. Lett. **43**, 1954 (1979).
[7] S. Aubry and G. André, Ann. Isr. Phys. Soc. **3**, 18 (1980).
[8] J. Sokoloff, Phys. Rep. **126**, 189 (1985).
[9] R. B. Griffiths, Phys. Rev. Lett. **23**, 17 (1969).
[10] B. M. McCoy, Phys. Rev. Lett. **23**, 383 (1969).
[11] G. Roati, C. DErrico, L. Fallani, M. Fattori, C. Fort, M. Zaccanti, G. Modugno, M. Modugno, and M. Inguscio, Nature (London) **453**, 895 (2008).
[12] N. Armitage, E. Mele, and A. Vishwanath, Rev. Mod. Phys. **90**, 015001 (2018).
[13] E. Fradkin, Phys. Rev. B **33**, 3263 (1986).
[14] P. Goswami and S. Chakravarty, Phys. Rev. Lett. **107**, 196803 (2011).
[15] K. Kobayashi, T. Ohtsuki, K.-I. Imura, and I. F. Herbut, Phys. Rev. Lett. **112**, 016402 (2014).
[16] B. Sbierski, G. Pohl, E. J. Bergholtz, and P. W. Brouwer, Phys. Rev. Lett. **113**, 026602 (2014).
[17] B. Roy and S. Das Sarma, Phys. Rev. B **90**, 241112(E) (2014); **93**, 119911 (2016).
[18] R. Nandkishore, D. A. Huse, and S. L. Sondhi, Phys. Rev. B **89**, 245110 (2014).
[19] J. H. Pixley, P. Goswami, and S. Das Sarma, Phys. Rev. Lett. **115**, 076601 (2015).
[20] A. Altland and D. Bagrets, Phys. Rev. Lett. **114**, 257201 (2015).
[21] S. V. Syzranov, L. Radzihovsky, and V. Gurarie, Phys. Rev. Lett. **114**, 166601 (2015).
[22] S. V. Syzranov, V. Gurarie, and L. Radzihovsky, Phys. Rev. B **91**, 035133 (2015).
[23] B. Sbierski, E. J. Bergholtz, and P. W. Brouwer, Phys. Rev. B **92**, 115145 (2015).
[24] J. H. Pixley, P. Goswami, and S. Das Sarma, Phys. Rev. B **93**, 085103 (2016).
[25] M. Gärttner, S. V. Syzranov, A. M. Rey, V. Gurarie, and L. Radzihovsky, Phys. Rev. B **92**, 041406 (2015).
[26] S. Liu, T. Ohtsuki, and R. Shindou, Phys. Rev. Lett. **116**, 066401 (2016).
[27] S. Bera, J. D. Sau, and B. Roy, Phys. Rev. B **93**, 201302 (2016).
[28] H. Shapourian and T. L. Hughes, Phys. Rev. B **93**, 075108 (2016).
[29] A. Altland and D. Bagrets, Phys. Rev. B **93**, 075113 (2016).
[30] S. V. Syzranov, P. M. Ostrovsky, V. Gurarie, and L. Radzihovsky, Phys. Rev. B **93**, 155113 (2016).
[31] T. Louvet, D. Carpentier, and A. A. Fedorenko, Phys. Rev. B **94**, 220201 (2016).
[32] J. H. Pixley, D. A. Huse, and S. Das Sarma, Phys. Rev. X **6**, 021042 (2016).
[33] J. H. Pixley, D. A. Huse, and S. Das Sarma, Phys. Rev. B **94**, 121107 (2016).
[34] B. Sbierski, K. A. Madsen, P. W. Brouwer, and C. Karrasch, Phys. Rev. B **96**, 064203 (2017).
[35] J. H. Pixley, Y.-Z. Chou, P. Goswami, D. A. Huse, R. Nandkishore, L. Radzihovsky, and S. Das Sarma, Phys. Rev. B **95**, 235101 (2017).
[36] V. Gurarie, Phys. Rev. B **96**, 014205 (2017).
[37] J. H. Wilson, J. H. Pixley, P. Goswami, and S. Das Sarma, Phys. Rev. B **95**, 155122 (2017).
[38] J. H. Wilson, J. H. Pixley, D. A. Huse, G. Refael, and S. D. Sarma, arXiv:1801.05438.
[39] S. Syzranov and L. Radzihovsky, Annu. Rev. Condens. Matter Phys. **9**, 35 (2018).
[40] W. De Roeck and F. Huveneers, Phys. Rev. B **95**, 155129 (2017).
[41] Y. Wang and S. Chen, Phys. Rev. A **95**, 053634 (2017).
[42] V. Khemani, D. N. Sheng, and D. A. Huse, Phys. Rev. Lett. **119**, 075702 (2017).
[43] A. Weiße, G. Wellein, A. Alvermann, and H. Fehske, Rev. Mod. Phys. **78**, 275 (2006).

[44] See Supplemental Material at http://link.aps.org/supplemental/10.1103/PhysRevLett.120.207604 for a discussion of finite size effects, the momentum space inverse participation ratio, the inversion of the semimetal, transport, and the Anderson localization transition at larger quasiperiodicity.
[45] H. Fehske and R. Schneider, *Computational Many-Particle Physics* (Springer, New York, 2008).
[46] T. Devakul and D. A. Huse, Phys. Rev. B **96**, 214201 (2017).
[47] J.-H. Jiang, Phys. Rev. A **85**, 033640 (2012).
[48] K. Sun, W. V. Liu, A. Hemmerich, and S. D. Sarma, Nat. Phys. **8**, 67 (2012).
[49] T. Dubcek, C. J. Kennedy, L. Lu, W. Ketterle, M. Soljacic, and H. Buljan,Phys. Rev. Lett. **114**, 225301 (2015).
[50] X. Li and S. D. Sarma, Nat. Commun. **6**, 7137 (2015).